Accelerating and abruptly autofocusing matter waves

Nikolaos K. Efremidis* and Vassilis Paltoglou
Department of Applied Mathematics, University of Crete, 71409 Heraklion, Crete, Greece

Wolf von Klitzing
Institute of Electronic Structure and Laser, Foundation for Research and Technology - Hellas, 71110 Heraklion, Crete, Greece
(Received 20 March 2013; published 30 April 2013)

We predict that classes of coherent matter waves can self-accelerate without the presence of an external potential. Such Bose-Einstein condensates can follow arbitrary power-law trajectories and can also take the form of diffraction-free Airy waves. We also show that suitably engineered radially symmetric matter waves can abruptly autofocus in space and time. We suggest different schemes for the preparation of the condensate using laser beams to imprint an amplitude or a phase pattern onto the matter wave. Direct and Fourier space generation of such waves is discussed using continuous and binary masks as well as magnetic mirrors and lenses. We study the effect of interactions and find that independently of the type and strength of the nonlinearity, the dynamics are associated with the generation of accelerating matter waves. In the case of strong attractive interactions, the acceleration is increased while the radiation reorganizes itself in the form of soliton(s).

DOI: 10.1103/PhysRevA.87.043637 PACS number(s): 03.75.Kk, 05.30.Jp

I. INTRODUCTION

The realization of Bose-Einstein condensation in weakly interacting atomic gases offers the exciting possibility of observing quantum phenomena on a macroscopic scale. Such a behavior was first predicted by Bose and Einstein [1,2]. However, its experimental observation in dilute gases had to wait many decades until the arrival of laser cooling [3,4]. Since then, BEC has attracted a lot of attention in connection with the diverse physical phenomena that arise from the dual (quantum and wave) character of the system.

A major opportunity is to build applications which exploit the induced dynamic behavior of Bose-Einstein condensates (BECs). Over the years, a sophisticated arsenal of matter-wave tools has been developed. Examples include optical mirrors [5], lenses [6–8], as well as coherent atomic tunneling structures [9], waveguides [10], and lattices [11]. Coherent matter-wave structures such as, for example, dark solitons [12] and optical vortices [13] have been produced using phase engineering of the matter-wave form.

In this work, we show that the trajectory of a matter wave can follow an accelerating path in the absence of any external potential. We present experimentally viable methods to prepare such coherent structures and analyze their dynamic behavior even in the presence of nonlinearities. The best known example of an accelerating wave is the Airy wave packet, which is a nonspreading solution of the Schrödinger equation that follows a parabolic trajectory [14]. Interestingly enough, the Airy wave is proven to be the only nonspreading solution (whose density remains invariant as it evolves and whose spatial profile decays to zero in its wings) of the potential-free Schrödinger equation in one spatial dimension [15]. Note that a "perfect" Airy wave carries infinite power and thus is not physically realizable.

Such accelerated beams have recently attracted much attention in optics. The interest in such waves was triggered when it was found that exponentially truncated—and thus finite power—Airy beams can be generated in the Fourier space by applying a cubic phase mask to a Gaussian beam [16]. This led to a large amount of activity in recent years including the finding of different families of curved beams such as nonparaxial curved beams [17], curved Bessel beams that follow arbitrary trajectories [18,19], and nonlinear curved beams [20–22], and applications in diverse areas such as filamentation [23] and particle manipulation [24] (see also the review article [25]). In higher dimensions, abruptly autofocusing waves are radially symmetric configurations of accelerating beams with the particularly interesting property to abruptly focus its energy at the focal point [26] (as compared to the Lorenzian intensity distribution around the focus of a Gaussian beam passing through a lens). Abruptly autofocusing waves have been experimentally observed in connection with applications in material ablation [27] and particle manipulation [28]. Theoretical techniques are available for the generation of different classes of such beams in the Fourier space [29,30].

The purpose of this work is to show that the wave function of a BEC can follow arbitrary convex trajectories provided that the initial state is carefully manipulated. Furthermore, we show that it is possible to generate abruptly autofocusing matter waves: BECs whose radially symmetric structure results in an abrupt focus in time. For the generation of such accelerating matter waves, a manipulation of the amplitude and/or the phase of the mean-field wave function is required. We suggest a number of different experimental techniques that can be utilized to this end. Finally, we study the effect of nonlinearity on the dynamics of accelerating matter waves for both attractive and repulsive interactions, and in either case we consider the weakly and strongly interacting regime. Our simulations show that in all of these cases, the matter waves exhibit accelerating trajectories. The strong attractive interactions lead to more complex dynamics and, in particular, to increased acceleration and shedding of solitons.

II. MEAN-FIELD DYNAMICS

Let us start our analysis by considering the dynamics of a BEC in the presence of a potential $V_0(\mathbf{r}',t')$ as described by

*nefrem@tem.uoc.gr

 ©2013 American Physical Society

the Gross-Pitaevskii equation,

$$i\hbar\frac{\partial\Psi}{\partial t'}=\left[-\frac{\hbar^2}{2m}\nabla'^2+V_0(\mathbf{r}',t')+g|\Psi|^2\right]\Psi, \tag{1}$$

where $\nabla'^2=\partial_{x'x'}+\partial_{y'y'}+\partial_{z'z'}$, Ψ is the wave function, $\hbar$ is Planck's constant, $g=4\pi a_s\hbar^2/m$ is the nonlinear coefficient that takes into account the mean field produced by the other bosons, m is the atomic mass, and a_s is the s-wave scattering length. The total potential

$$V_0(\mathbf{r}',t')=\frac{m}{2}\left(\omega_x^2x'^2+\omega_y^2y'^2+\omega_z^2z'^2\right)+\tilde{V}(\mathbf{r}',t') \tag{2}$$

can be decomposed into a harmonic term and an additional potential $\tilde{V}$, which we will subsequently specify. For pancake-shaped ($\omega_z=\omega_\perp\gg\omega_x,\omega_y$) and cigar-shaped ($\omega_y=\omega_z=\omega_\perp\gg\omega_x$) harmonic potentials, our model equation can be asymptotically reduced to a lower-dimensional one, which is substantially simpler to analyze (see, for example, [31–33]). In the weak-interaction limit [31,33], the main requirement is that the ground-state harmonic-oscillator energy in the direction of tight confinement is much larger than the interaction energy. As a result of this assumption, in the case of a cigar-shaped harmonic potential term, we can decompose the wave function into

$$\Psi(\mathbf{r}',t')=A(x',t')U(y',z'), \tag{3}$$

where

$$U(y',z')=\left(\frac{m\omega_\perp}{\pi\hbar}\right)^{1/2}\exp\left[-\frac{m\omega_\perp}{2\hbar}(y'^2+z'^2)\right]$$

is the ground-state eigenfunction of the quantum harmonic-oscillator potential with an eigenvalue $E=\hbar\omega_\perp$. By substituting Eq. (3) into Eq. (1), applying the transformation $A\to Ae^{-iEt'/\hbar}$, multiplying with $U(y',z')$, and integrating over the y'–z' plane, we obtain

$$i\hbar\frac{\partial A}{\partial t'}=-\frac{\hbar^2}{2m}\frac{\partial^2A}{\partial x'^2}+V(x',t')A+\frac{m\omega_x^2x'^2}{2}A+\tilde{g}|A|^2A, \tag{4}$$

where $\tilde{g}=2\hbar\omega_\perp a_s$. The same analysis can also be applied for pancakelike condensates. In particular, we derive an equation similar to Eq. (4) with a two-dimensional diffraction operator and a nonlinear coefficient that is given by $\tilde{g}=a_s\sqrt{8\pi\omega_x\hbar^3/m}$. We introduce normalized coordinates $t=t'\omega$, $\{x,y\}=\{x',y'\}/L$, $\psi=L_0^{d/2}A$, where $d=1$ for a cigar-shaped condensate and $d=2$ for a pancake-shaped condensate. We choose to fix the diffraction coefficient to $1/2$ by requiring $L=\sqrt{\hbar/m\omega}$, leading to

$$i\frac{\partial\psi}{\partial t}=-\frac{1}{2}\frac{\partial^2\psi}{\partial x^2}+\Omega_x^2x^2\psi+V(x,t)\psi+g_1|\psi|^2\psi, \tag{5}$$

where, for cigar-type condensates,

$$\Omega_x=\frac{\omega_x}{2^{1/2}\omega},\quad g_1=\frac{2a_s\omega_\perp}{L_0\omega},\quad V(x)=\frac{1}{\hbar\omega}\tilde{V}(Lx), \tag{6}$$

and for pancake-type condensates,

$$\Omega_{\{x,y\}}=\frac{\omega_{\{x,y\}}}{2^{1/2}\omega},\quad g_2=\sqrt{8\pi}\frac{La_s}{L_0^2}\sqrt{\frac{\omega_\perp}{\omega}},\quad V=\frac{\tilde{V}(Lx,Ly)}{\hbar\omega}. \tag{7}$$

In the strongly interacting, high-density limit, the effective dynamics of cigar-shaped and pancake-shaped condensates are modified [32]. Following the relevant algebra, we find that only the nonlinear term of Eq. (4) is modified. In particular, in the case of cigar-shaped condensates, the effective nonlinearity is quadratic, $g_1|\psi|\psi$, while in the case of pancake-shaped condensates, the nonlinearity takes the form $g_2|\phi|^{4/3}\psi$, where the normalized nonlinear coefficients are given by

$$g_1=\sqrt{\frac{9}{2}}\left(\frac{a_s}{L_0}\right)^{1/2}\frac{\omega_\perp}{\omega} \tag{8}$$

and

$$g_2=\frac{5\pi^{1/3}}{2}\left(\frac{L}{L_0}\right)^{2/3}\left(\frac{a_s}{L_0}\right)^{2/3}\left(\frac{\omega_\perp}{\omega}\right)^{2/3}. \tag{9}$$

Note that in our examples time is scaled as $1/\omega$. Values of ω of the order of 10^3 rad/s thus yield a time scale of 1 ms.

In the rest of the section, we are going to discuss different methods for generating the amplitude and phase masks for the condensate (see Fig. 1). We apply an additional potential $V(x,t)$ to the matter wave, e.g., in the form of a (non)resonant light pattern. We do so on a time scale $t\ll\Omega_x^{-1}$ such that both the harmonic potential and the kinetic terms can be ignored in Eq. (5). We then let the matter wave evolve freely along the x direction in the absence of any potential in that direction. The additional potential $\tilde{V}(x,t)$ is used for the preparation of the amplitude and/or phase distribution of the initial mean-field wave function. In particular, when we expose the BEC to an off-resonant laser with intensity $I(x',y')$ and pulse duration T, an effective potential of the form

$$\tilde{V}(x',y')=\frac{\hbar\Gamma^2}{8\Delta}\frac{I(x',y')}{I_0}$$

is applied, where Γ is the transition line width, I_0 is the saturation intensity, and Δ is the detuning of the laser from the atomic resonance. Assuming that the time interval T is small enough so that the atomic motion is negligible, the condensate accumulates a phase [12]

$$\phi(x,y)=-\frac{\Gamma^2T}{8\Delta\omega}\frac{I(Lx,Ly)}{I_0}. \tag{10}$$

The spatial intensity profile of the laser beam $I(x',y')$ applied to the BEC can be shaped by optical elements such

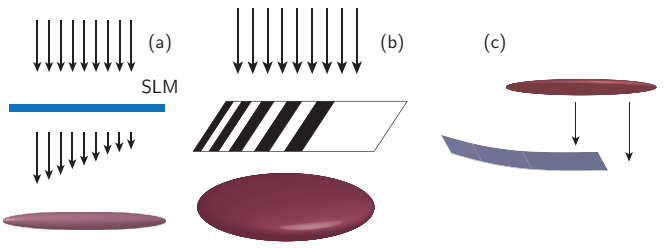

FIG. 1. (Color online) Different configurations for the generation of accelerating matter waves. (a) A phase or amplitude profile is imprinted to the BEC by exposing it to a pulsed off-resonance or on-resonance laser beam, respectively, that passes through an amplitude spatial light modulator. (b) An aperture is intervened between the laser pulse and the matter wave. (c) A part of the condensate is reflected by a curved magnetic mirror.

as a photographic film or a spatial light modulator (SLM), as shown in Fig. 1(a). The SLM offers the advantage of applying multiple light pulses of different spatial distributions in time by the frame refresh rate. The cost for this flexibility is that the resulting laser pattern is pixelized, which, thus far, has not been a limiting factor in the observation of complicated wave structures in optics [25]. Figure 1(b) shown a binary aperture, which is used to block a part of the laser beam according to its spatial position (x,y). By controlling the pulse duration, pulse intensity, and detuning, we can apply a phase distribution consisting of regions with phases 0 and π. The same methods can also be used to control the amplitude profile of the matter waves. Specifically, it has been demonstrated that an on-resonance laser beam ($\Delta = 0$) can remove atoms from the condensate and thus suppress the local atom density [34].

The phase of the condensate can also be manipulated by applying pulsed magnetic fields [6,7]. This is particularly useful for the creation of a focusing parabolic phase pattern [35].

Another configuration for the generation of accelerating matter waves is illustrated in Fig. 1(c). In this case, the matter wave is falling along the z direction due to gravity. A part of the matter wave faces a magnetic mirror and bounces back. Thus the magnetic mirror acts as an amplitude mask that eliminates the part of the wave that does not fall in the mirror. In addition, the mirror is curved and reshapes the wave front. By engineering the curvature of the mirror, an arbitrary phase $\phi(x,y)$ can be accumulated at each position (x,y) of the reflected matter wave. This process can result in the generation of BECs that accelerate in the transverse (x,y) plane.

III. GENERATION OF ACCELERATING MATTER WAVES

In this section, we are going to describe different methods for the generation of matter waves that follow generic power-law trajectories including Airy-type matter waves, as well as abruptly autofocusing waves. At first, we will limit our analysis to the case where the atom density is small enough and thus the interaction term can be ignored in the dynamics of the condensate. This condition can easily be fulfilled by reducing the density of the condensate through expansion. Alternatively, the interactions can be significantly reduced through Feshbach resonances. The effect of nonlinearity in the dynamics of accelerated matter waves will be treated in Sec. IV. As we will see, even in the presence of moderate or strong nonlinearity (attractive or repulsive), the dynamics can still maintain or even enhance the characteristic accelerating behavior of the linear limit.

A. Fourier space generation using continuous phase masks

Matter-wave optics, just like its photonic counterpart, allows one to generate the Fourier image of an object simply by applying a focusing lens [35]. We can, therefore, engineer our matter wave in Fourier space, where the optical distances involved are more readily accessible. This can be achieved by the use of two subsequent laser pulses passing through a programmable amplitude SLM or by one laser pulse plus a magnetic field for matter-wave phase imprinting as discussed above. In particular, we consider the dynamics of Eq. (5), which, in the limit of low atom density, is described by the Fresnel-type integral

$$\psi(x,t) = \frac{1}{(2i\pi t)^{1/2}} \int_{\mathbb{R}} e^{i(x-\xi)^2/(2t)} \psi(\xi,0) d\xi. \tag{11}$$

At $t = 0$, a power-law phase of the form

$$\phi_1(\xi) = -\mathrm{sgn}(\xi)|\xi|^\beta/\beta \tag{12}$$

is applied to the matter wave, whereas at $t = t_f$, an additional parabolic phase

$$\phi_2(\xi) = -\xi^2/(2t_f) \tag{13}$$

is imprinted. In Eq. (12), β is the phase exponent and γ defines a transverse scaling of the matter wave's phase. The parabolic phase is used to emulate the role of a Fourier transform which is spontaneously generated at $t = 2t_f$. In particular, the scaling between the Fourier transform of the initial profile and the amplitude of the matter wave at $t = 2t_f$ satisfies

$$\psi(x, t = 2t_f) = \frac{1}{(2i\pi t_f)^{1/2}} \tilde{\psi}\left(\frac{x}{t_f}, t = 0^+\right), \tag{14}$$

where $\tilde{\psi}(x,0^+)$ is the Fourier transform of the matter wave at $t = 0$ after the phase profile $\phi_1(x)$ is imprinted. Note that we use the following definition for the Fourier-transform pair:

$$\tilde{u}(k) = \int_{-\infty}^{\infty} e^{-ikx} u(x) dx, \quad u(x) = \frac{1}{2\pi} \int_{-\infty}^{\infty} e^{ikx} \tilde{u}(k) dk.$$

Of particular interest is the special case where a cubic phase ($\beta = 3$) is imprinted to the condensate. Specifically, the following exact relation holds for the Fourier transform of a cubic phase that is shifted in the complex plane as $k \to k + i\alpha$ [16]:

$$u(x) = \frac{1}{2\pi} e^{i(-x+i\alpha)^3/3}, \quad \tilde{u}(k) = e^{\alpha k} \mathrm{Ai}(k). \tag{15}$$

By combining Eq. (15) with Eq. (14), we conclude that an Airy wave of the form

$$\psi(x, t = 2t_f) = \frac{A}{(2i\pi t_f)^{1/2}} \mathrm{Ai}\left(\frac{\gamma x}{t_f}\right) e^{\alpha x/t_f} \tag{16}$$

can be generated at $t = 2t_f$ if the initial state [with the imprinted phase $\phi_1(x,y)$] has the form

$$\begin{aligned} \psi(\xi, t = 0^+) &= \frac{A}{2\pi\gamma} e^{i(-\xi+i\alpha)^3/3\gamma^3} \\ &= \frac{A}{2\pi\gamma} e^{-i(\xi^3/3+\xi\alpha^2)/\gamma^3} e^{-\xi^2\alpha/\gamma^3+\alpha^3/3\gamma^3}. \end{aligned} \tag{17}$$

When $\alpha = 0$, the initial condition represents a plane wave with a cubic phase modulation. At $t = 2t_f$, the matter wave is transformed to an ideal Airy wave [Eq. (16)]. This latter solution requires an infinite number of atoms and thus is physically unrealizable. The introduction of the apodization or truncation factor $\alpha > 0$ provides a mechanism to resolve this problem. This becomes apparent by examining the right-hand side of the initial condition term by term. The phase of Eq. (17) consists of a cubic and an additional linear term. The linear phase term is not important in the dynamics of the BEC mainly because it describes a lateral shift of the Airy wave at $t = 2t_f$. In addition, this term should be small provided that the truncation coefficient α is also small. The amplitude

is given by the last exponent of Eq. (17) and consists of a Gaussian distribution (leading to a finite atom number) and a amplitude scaling term (a term that does not involve ξ). This amplitude profile is the natural lowest-order mode of a BEC in a relatively strong harmonic potential. Note that different truncation functions can still lead to the generation of such accelerated matter waves, which, however, might not be analytically described in a closed form. The (normalized) number of atoms of the truncated Airy wave can be easily computed from the initial Gaussian distribution to be

$$N = \int_{-\infty}^{\infty} |\psi(\xi,t)|^2 d\xi = \frac{e^{\frac{2\alpha^3}{3\gamma^3}}}{\sqrt{32\alpha\pi^3\gamma}}.$$

More importantly, the dynamics of an Airy wave follows a parabolic trajectory as it is described by the following exact solution [16]:

$$\psi(x,t) = \mathrm{Ai}\left(cx - \frac{c^4t^2}{4} + iact\right)\exp\left[a\left(x - \frac{c^3t^2}{2}\right) + \frac{it}{2}\left(a^2 + c^3x - \frac{1}{6}c^6t^2\right)\right], \tag{18}$$

where

$$a = \alpha/t_f, \quad c = \gamma/t_f.$$

In Eq. (18), time is shifted by $2t_f$ (we will also use similar time shifts below to simplify the resulting expressions). In the limit $a \to 0$, this solution becomes a diffraction-free solution of the Schrödinger equation [14], meaning that the density profile does not change with time. The Airy wave form is actually the only diffraction-free solution of the Schrödinger equation in one dimension and it follows the parabolic trajectory $x = ct^2/4$. Even for $\alpha > 0$, the exact solution maintains the diffraction-free characteristics of the Airy wave for large evolution times.

We can obtain generalized power-law trajectories by constructing the following initial condition:

$$\psi(\xi, t = 2t_f) = A(\xi)e^{i\phi_1(\xi)}, \tag{19}$$

where $\phi_1(\xi)$ is given by Eq. (12). Using a stationary phase approximation and Eq. (14) that relates the Fourier transform and the wave function at $t = 2t_f$, we conclude that

$$\psi(x,2t_f) = \left(\frac{b-1}{it_f}\right)^{1/2} \frac{2ct_f}{(-cx)^{\frac{2-b}{2}}} A[ct_f(-cx)^{b-1}] \times \cos\left[\frac{(-cx)^b}{b} - \frac{\pi}{4}\right], \tag{20}$$

where we have defined

$$b = \beta/(\beta - 1).$$

The above formula is an excellent approximation of the exact solution for $x\gamma/t_f < -1$. The sinusoidal interference pattern is generated from the mixing of the two stationary phase points that originate from opposite ξ ($\pm\xi$) and arrive at the same x at $t = 2t_f$. In the limiting case where $\beta = 3$, Eq. (20) is identical to the asymptotic expression of the Airy wave [Eq. (18) with $t = 0$] that is described by a phase exponent $3/2$ and an amplitude modulation proportional to $1/(-x)^{1/4}$. Furthermore, a Gaussian truncation function $A(\xi)$ results in an exponential apodization, as expected. Note that since the initial condition scales with γ as ξ/γ and the resulting pattern scales as $x\gamma$, a broader initial BEC results in a narrower accelerating matter wave. This result is trivially expected because these two functions are related through a Fourier transform. However, this property can be utilized to generate matter waves that are smaller than the diffraction limit that is imposed to light waves.

From this point on, we consider that $t = 2t_f$ is shifted to $t = 0$ for convenience. We evaluate the Fresnel integral (11) with an initial condition that is given by Eq. (20) using a stationary phase approximation. The trajectory of the matter wave is then derived by requiring second-order stationarity of the phase. Furthermore, we can parametrically determine the trajectory of the matter wave as a function of the initial coordinate ξ as

$$(x,t) = \left[-\frac{(2-b)\xi}{(b-1)}, \frac{(-c\xi)^{2-b}}{c^2(b-1)}\right]. \tag{21}$$

We can eliminate ξ from Eq. (21), leading to the power-law expression

$$x = (2-b)(b-1)^{\frac{b-1}{2-b}}c^{\frac{b}{2-b}}t^{\frac{1}{2-b}} = (q-1)^{q-1}c^{2q-1}\left(\frac{t}{q}\right)^q, \tag{22}$$

where $q = 1/(2-b)$. Setting the values of β between 2 and infinity, then $1 < b < 2$ and the power-law trajectory exponent ranges between 1 and infinity. In the limiting case $b = 1$, the phase chirp becomes zero and thus the caustic disappears. On the other hand, for $b = 2$, the caustic collapses to a focus, in which case the presence of additional aberrations leads to a fold-type catastrophe. We can directly express the phase exponents of the wave at $t = 0$ and at $t = 2t_f$ (b and β) as a function of the exponent of the accelerating trajectory q as

$$b = \frac{2q-1}{q}, \quad \beta = \frac{2q-1}{q-1}.$$

In Fig. 2, we present typical examples of different power-law trajectories that are generated by the procedure described above. In particular, in Figs. 2(a) and 2(b), we see the generation of Airy matter waves that follow quadratic trajectories. In Figs. 2(c) and 2(d), we depict matter waves with a cubic trajectory and a power-law trajectory with an exponent $q = 2.5$, respectively. As can be seen from Eq. (22) for a fixed value of q (and thus β), the trajectory of the matter wave depends solely on the parameter $c = \gamma/t_f$. Thus, we have the flexibility to generate the desired matter-wave trajectory for different values of γ and t_f, provided that they satisfy the linear condition $\gamma = ct_f$.

B. Fourier space generation using binary phase masks

In this section, we show that it is possible to generate accelerating matter waves by applying a binary phase mask ($\phi = 0$ or π) to the BEC. Let us assume that at $t = 0$ the phase that is imprinted to the condensate is given by the relation

$$\hat{\phi}_1 = \frac{\pi}{2}(1 - \mathrm{sgn}\{\cos[\kappa x + \phi_1(x)]\}). \tag{23}$$

In Eq. (23), $\phi_1(x)$ is the phase that we would like to impose, which is given by Eq. (12), and κ is a parameter that is used

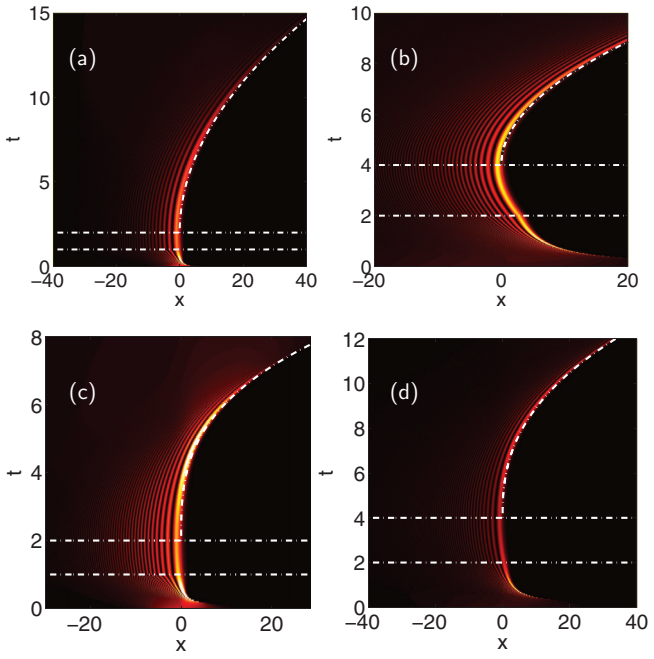

FIG. 2. (Color online) Accelerating matter-wave generation via two subsequent continuous phase imprints. (a), (b) A parabolic-trajectory Airy matter wave is generated with (a) $\gamma = 1$, $t_f = 1$, and $\alpha = 0.03$ and (b) $\gamma = 3$, $t_f = 2$, and $\alpha = 0.03$ in Eq. (17). An accelerating BEC is shown that follows (c) a cubic trajectory with $\alpha = 0.01$, $\beta = 5/2$, $\gamma = 1$, $t_f = 1$ and (d) a power-law trajectory with exponent $q = 2.5$ and $\alpha = 0.01$, $\beta = 8/3$, $\gamma = 2$, $t_f = 2$. The accelerating caustics are depicted by the curved lines, while the horizontal lines correspond to $t = t_f$ and $t = 2t_f$. Note that for simplicity, the truncation function in all cases presented here is taken to be same as in the exponentially apodized Airy waves [Eq. (17)], i.e., it has the form $\exp(-\alpha x^2/\gamma^3)$.

to separate the diffraction orders. Assuming that the initial amplitude profile is given by $A(x)$, then after the phase $\hat{\phi}_1$ is applied we have

$$\psi(x,t=0^+) = A(x)\mathrm{sgn}\{\cos[\kappa x + \phi_1(x)]\} = A(x)\sum_{n\neq 0}\mathrm{sinc}\left(\frac{\pi n}{2}\right)e^{in[\kappa x+\phi_1(x)]}, \quad (24)$$

where on the right-hand side of Eq. (24) the matter-wave profile is expressed as a series expansion. The values of n in the above sum are called the diffraction orders. Interestingly enough, the zero diffraction order is zero (along with the rest of the even diffraction orders, $n = 2m$). Due to symmetry, the terms n and $-n$ generate mirror-symmetric wave profiles, and for this reason $\psi(x,t)$ is an even function of x [provided that $A(x)$ is also an even function of x]. Thus, we only need to analyze the positive diffraction orders. In particular, we isolate the first diffraction order ($n = 1$)

$$\psi_1(x,t=0^+) = \frac{2}{\pi}A(x)e^{i\kappa x+i\phi_1(x)}. \quad (25)$$

We note that Eq. (25) is identical to the generic profile of Eq. (19) with the addition of the linear phase term κx. The strongest perturbation to the first diffraction order is the third diffraction order term that is given by

$$\psi_3(x,t=0^+) = -\frac{2}{3\pi}A(x)e^{3i\kappa x+3i\phi(x)}. \quad (26)$$

The maximum density of the latter is nine times smaller than the density of the first diffraction order and thus can be considered as a perturbation. At $t = t_f$, a focusing phase is applied to the condensate. The phase can be either continuous parabolic or binary (Fresnel lens). In the case of a continuous parabolic potential, the analysis of the previous section can be directly repeated with the only difference that the initial profile given by Eq. (25) has an additional linear phase term (κx), which results in a spatial lateral shifting of the matter wave at $t = 2t_f$ along the x direction. Equation (20) can also be utilized here with the additional transformation $\gamma x/t_f \to \gamma x/t_f - \kappa$, which quantifies the lateral shifting at $t = 2t_f$ to $\kappa t_f/\gamma$. In Fig. 3(a), the generation of such an Airy wave is depicted. As expected, the resulting wave amplitude profile is even, due to the generation of an additional Airy wave (with $n = -1$) that moves in the opposite direction. We have chosen the phase $\phi_1(x)$ to have the opposite sign as compared to Eq. (12) in order to generate accelerating waves that propagate towards each other (instead of moving away from each other). Thus, we ensure minimum interference with the higher diffraction orders that are associated with a larger lateral shift. After some evolution time, we observe the autofocusinglike collision of the two "facing each other" Airy beams. In Fig. 3(c), we see an accelerating wave generated with the same procedure that follows a cubic trajectory.

Instead of using a parabolic phase, we can also utilize a binary Fresnel-zone-type phase to emulate the focus,

$$\phi_2(x) = \frac{\pi}{2}\left\{1 - \mathrm{sgn}\left[\cos\left(\frac{x^2}{2f}\right)\right]\right\}.$$

The action of the Fresnel-zone-plate-type phase imprinting can be analyzed by noting that we can express the matter-wave amplitude profile after the phase ϕ_2 is applied as

$$\psi(x,t=t_f^+) = \psi(x,t=t_f^-)U_2(x),$$

where $U_2(x)$ can be decomposed in the following series:

$$U_2(x) = \mathrm{sgn}\left[\cos\left(\frac{x^2}{2t_f}\right)\right] = \sum_{n\neq 0}\mathrm{sinc}\left(\frac{\pi n}{2}\right)e^{inx^2/(2t_f)}. \quad (27)$$

Each nonzero (odd-n) term is a focus with focal time $-t_f/n$. For positive values of n, the focal time is negative, meaning that the rays diverge as time increases and thus only negative n result in real, positive-time foci. The $n = -1$ term is the strongest focus associated with the longest focal time (equal to t_f), which we make use of in our formulas. Typical examples of the generation of accelerating matter waves using the described procedure are shown in Figs. 3(b) and 3(d), which follow parabolic and cubic trajectories, respectively. We can directly compare the quality of the ideal parabolic focus with the Fresnel-zone-plate focus by comparing Figs. 3(a) and 3(c) with Figs. 3(b) and 3(d). In the case of a Fresnel-zone-type focus, the higher diffraction orders, associated with higher-order foci at $t = -t_f/n, n = -3, -5, \ldots$, can interfere with the fundamental focus. We observe this type of interference,

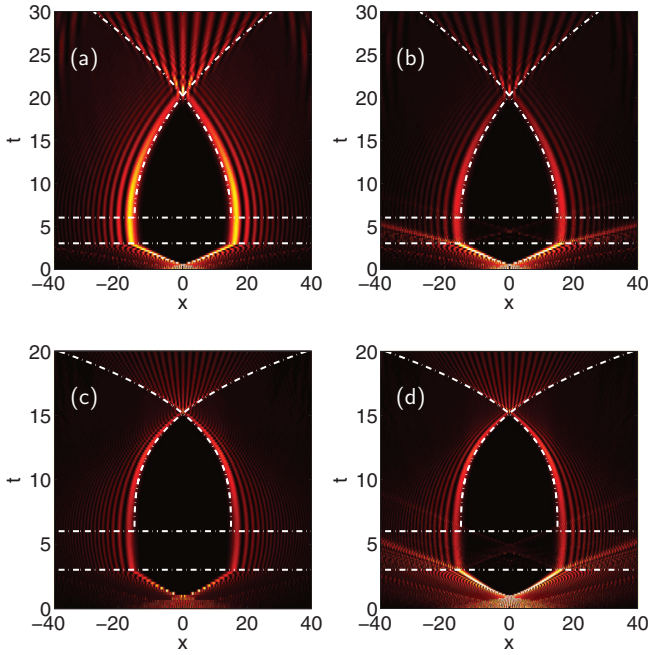

FIG. 3. (Color online) Accelerating matter waves generated in the Fourier space by the use of binary phase imprints. In the top and bottom of the figure, the trajectories are quadratic and cubic, respectively. On the left, the matter waves are generated via a binary phase and a subsequent continuous parabolic phase, whereas on the right, the focusing phase is emulated by an equivalent of a Fresnel zone plate. (a), (b) $\gamma = 2$, $t_f = 3$, $\alpha = 0.1$, $\beta = 3$, $\kappa = 5$; (c), (d) $\gamma = 2$, $t_f = 3$, $\alpha = 0.02$, $\beta = 5/2$, $\kappa = 5$. The accelerating caustics are depicted by the curved lines, while the horizontal lines correspond to $t = t_f$ and $t = 2t_f$. The amplitude profile of the initial condition has the form $\exp(-\alpha x^2/\gamma^3)$.

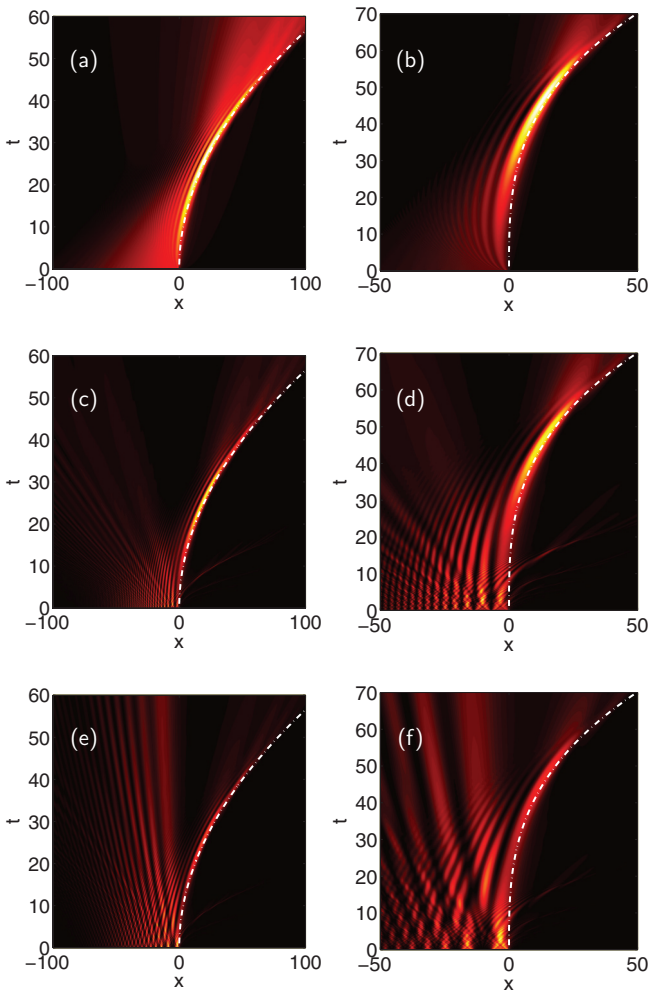

FIG. 4. (Color online) Direct matter-wave generation. In the top, middle, and bottom panels, the initial conditions are provided by, Eqs. (28), (29), (30), and (31), respectively. In the left and right panels, the resulting trajectories are parabolic and cubic and are given by Eq. (22) with $b = 3/2$, $c = 1/2$ and $b = 5/3$, $c = 1/4$, respectively. The amplitude function in all cases is $A(x) = \exp[-(x/60)^2]$.

which, however, is limited to evolution times between t_f and $2t_f$. Note that in the figures only the first two nonzero diffraction orders are visible. For even larger propagation distances, the different diffraction orders become spatially separated due to different propagation velocities.

C. Direct generation of accelerating waves

We are now going to study the direct generation of accelerating BECs by the use of amplitude and/or phase masks that are applied at $t = 0$. An efficient method, in terms of the quality of the resulting accelerating matter-wave profile, is to apply an amplitude truncation that removes the condensate for $x > 0$ and simultaneously phase imprints the matter wave in the region $x < 0$. An alternative configuration with the same effective result is shown in Fig. 1(c). In this figure, a part of the condensate ($x < 0$) bounces back from a curved magnetic mirror that is designed to provide the desired phase pattern, while the remaining part of the condensate ($x > 0$) is separated (see, e.g., [5,8]). The resulting initial profile of the condensate then becomes

$$\psi(x,t=0) = A(x)H(-x)e^{i\phi(x)}, \tag{28}$$

where the phase is given by

$$\phi(x) = -\frac{(-cx)^b}{b}, \tag{29}$$

and $H(x)$ is the Heaviside step function. The above formula for the phase of the matter wave contains all the rays of Eq. (20) that evolve in the right direction and are responsible for the caustic generation. Thus, the resulting trajectory of the matter wave is still given by Eq. (22). In Fig. 4, we see typical examples of such waves. In Fig. 4(a), we have $b = 3/2$ and $c = 1/2$ with a Gaussian amplitude function $A(x) = \exp[-(x/60)^2]$. We use the same amplitude function $A(x)$ for the rest of the examples presented in Fig. 4. This case generates a quadratic term [Eq. (22)] associated with an Airy-type accelerating matter wave. In Fig. 4(b), we choose $b = 5/3$ and $c = 1/4$ that leads to a cubic BEC trajectory.

We also simulated the direct generation of accelerating matter waves by using the same procedure, but with a binary phase mask. In particular, the phase of the matter wave is taken to be

$$\phi(x) = \frac{\pi}{2}\left(1 - \mathrm{sgn}\left\{\cos\left[\frac{(-cx)^b}{b}\right]\right\}\right).$$

Using a series expansion, we can express the initial state as

$$\psi(x,z=0) = A(x)H(-x)\mathrm{sgn}\left\{\cos\left[\frac{(-cx)^b}{b}\right]\right\} = 2A(x)H(-x)\sum_{n>0}\mathrm{sinc}\left(\frac{\pi n}{2}\right)\cos\left[in\frac{(-cx)^b}{b}\right]. \quad (30)$$

Each of the terms in Eq. (30) generates an accelerating wave whose trajectory can be described by Eq. (22) with the substitution $c \to n^{1/b}c$ and $1 < b < 2$. Higher values of n result in stronger acceleration and faster wave bending. Thus, we expect that the higher diffraction orders, which are also weaker, are separated from the strongest first diffraction order in a relatively small amount of time. We can observe this effect in Figs. 4(c) and 4(d), where the first diffraction orders of the BEC follow the same parabolic and cubic trajectories as in Figs. 4(a) and 4(b), respectively. However, by carefully looking at the figures, we can also observe at least two more weaker diffraction orders ($n = 3,5$) that rapidly accelerate to the right. By comparing the top and middle rows of Fig. 4, we also observe that a part of the matter wave is moving to the left, which is generated from the diverging left-propagating rays of the sinusoidal wave form. After some evolution time, the resulting accelerating matter wave becomes identical to the one generated by the continuous phase approach, as can be seen by comparing Fig. 4(a) to Fig. 4(c) and Fig. 4(b) to Fig. 4(d).

Direct generation of accelerating matter waves can also be achieved by the use of a single amplitude truncation. Such a configuration can consist of a binary aperture that is intervened between a resonant laser and the matter wave. The transmitted part of the laser beam blows off the unwanted part of the condensate. After this process, the initial matter wave $\psi(x,t = 0^-) = A(x)$ takes the form $\psi(x,t = 0^+) = A(x)U(x)$, where

$$U(x) = \frac{1}{2}H(-x)\left(1 + \mathrm{sgn}\left\{\cos\left[\frac{(-cx)^b}{b}\right]\right\}\right). \quad (31)$$

A schematic illustration of the described process is shown in Fig. 1(c). The resulting wave profile $\psi(x,t = 0^+)$ is identical to the one of Eq. (30) with two main differences: (1) a coefficient $1/2$ that multiplies all the terms and, more importantly, (2) that the summation starts from $n = 0$. The zero diffraction order accounts for the diffraction of $A(x)H(-x)$. The zero diffraction order can interfere with the accelerating matter wave before, due to acceleration, the latter is shifted away from its initial position. For example, in Figs. 4(e) and 4(f), we see the dynamics of matter waves that follow parabolic and cubic trajectories with the same parameters as in Figs. 4(a) and 4(c), and 4(b) and 4(d), respectively. The difference in the dynamics between the second and the third rows in Fig. 4 is solely attributed to the zero diffraction order.

D. Abruptly autofocusing BEC

Finally, we briefly discuss the generation of abruptly autofocusing BEC. The techniques are similar to those used in the previous sections for the generation of accelerating matter waves. Direct generation of abruptly autofocusing waves is possible by using a magnetic mirror, such as the one shown in Fig. 1(c), for modulating the phase with an additional circular hole of radius r_0, so that only the region $r > r_0$ gets reflected. The equivalent, in this case of Eqs. (28) and (29), is

$$\psi(r,t=0) = A(r)H(r-r_0)e^{i\phi(r)}, \quad (32)$$

where the phase is given by

$$\phi(r) = \frac{[c(r-r_0)]^b}{b}. \quad (33)$$

In Fig. 5(a), we see a typical example of an abruptly autofocusing matter wave with $b = 3/2$ following a parabolic trajectory up until the radial caustic collapses in the focus. In Fig. 5(b), we show an example of direct generation of an abruptly autofocusing wave generated using a single intervening binary film and an on-resonance laser, such as the one shown in Fig. 1(b). The initial BEC profile is then given by $\psi(x,t) = A(x)U(x)$, where $U(x)$ is the equivalent of a Fresnel zone plate for abruptly autofocusing waves, and is given by

$$U(x) = \frac{H(r-r_0)}{2}\left[1 + \mathrm{sgn}\left(\cos\left\{\frac{[c(r-r_0)]^b}{b}\right\}\right)\right]. \quad (34)$$

Except from the fundamental focus, we can clearly observe the generation of higher diffraction order foci ($n = 3,5$) which are less intense and have shorter focusing times.

Finally, in Fig. 5(c), a typical example of abruptly autofocusing waves generated in the Fourier space, using a configuration similar to the one of Fig. 1(a), is shown. The main difference in the phase, as compared to Eq. (12), is the additional linear tilt, i.e.,

$$\phi(r) = \frac{1}{\beta}\left(\frac{r}{\gamma}\right)^\beta + \kappa r. \quad (35)$$

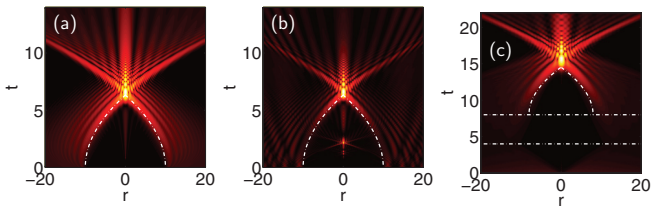

FIG. 5. (Color online) Abruptly autofocusing matter waves via (a) direct generation using Eqs. (32) and (33) with $c = 1$, $b = 3/2$, $r_0 = 10$ and (b) using Eq. (34) with the same parameters as in (a); (c) Fourier space generation using the imprinted phase of Eq. (35) with $\kappa = 2$, $\gamma = 3.47$, and $\beta = 3$. In all of the examples presented here, the initial amplitude profile is $\exp[-(r/40)^2]$. For illustration purposes, and since the density contrasts attained are large, we use a logarithmic scaling $\log(1 + |\psi|^2)$ for the wave. In all of the abruptly autofocusing examples presented here, the density contrasts attained are of the order of 10^4.

IV. NONLINEAR DYNAMICS

In this section, we focus on the effect of interactions giving rise to nonlinearities in the dynamics of the accelerated matter waves. In particular, we examine the dynamics of BECs in the presence of both attractive and repulsive interactions. In the case of relatively small or moderate interactions, the dynamics

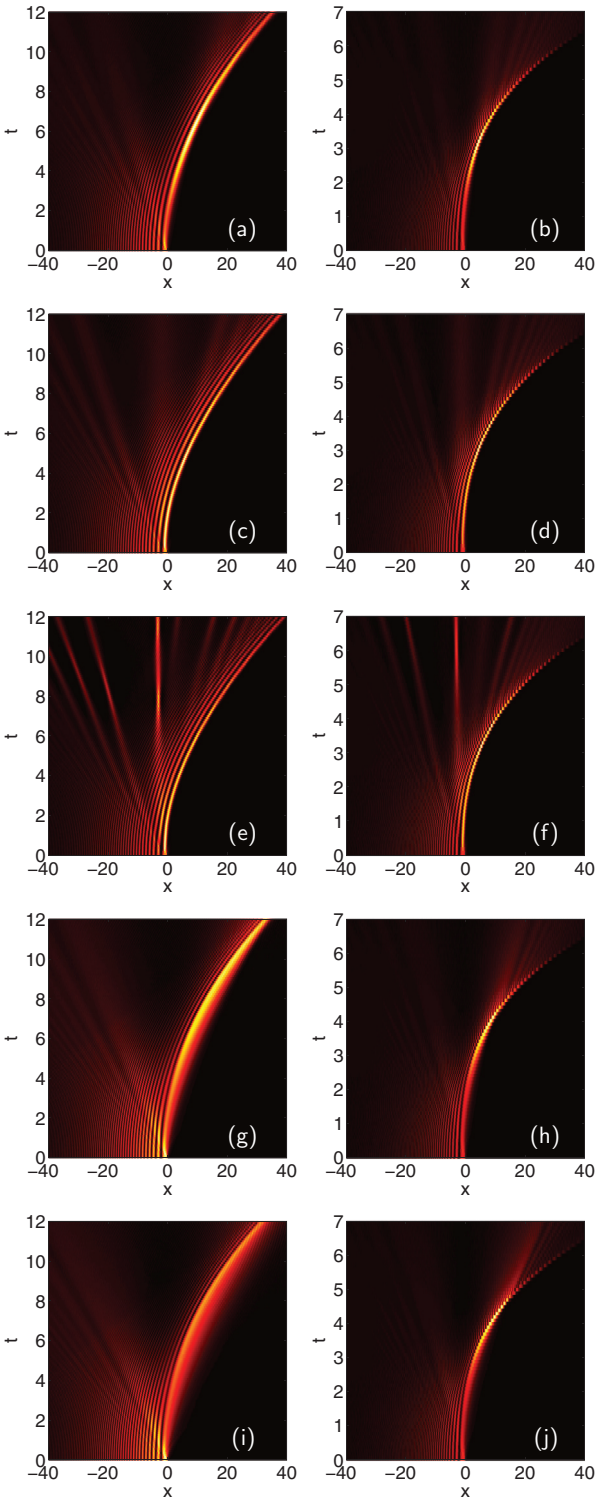

FIG. 6. (Color online) Typical examples of nonlinear propagation of accelerating matter waves. The initial condition is given by Eq. (36) where, in the left column, $b = 3/2$, generating a parabolic trajectory, while on the right column, $b = 5/3$, resulting in a cubic trajectory. In the top row [(a), (b)], the nonlinearity is switched off; in the second and third rows, the interactions are attractive; while in the fourth and fifth rows, the interactions are repulsive. In the second and fourth rows, we use a cubic nonlinearity [Eq. (5)] with $A = 1$, while in the third and fifth rows, a quadratic nonlinearity is considered with $A = 3$.

are fully described by the effective model of Eqs. (5) and (6), which has a cubic nonlinearity. On the other hand, in the case of cigar-shaped condensates with strong atom-atom interactions, the effective nonlinearity becomes quadratic and its coefficient is given by Eq. (9). To study the effect of nonlinearity in the dynamics of accelerating matter waves, we impose the same initial condition,

$$\psi(x,t=0) = BH(-x)\cos\left[\frac{(-x)^b}{b} - \frac{\pi}{4}\right]e^{0.03x}, \quad (36)$$

and change both the type and strength of the nonlinearity. In Eq. (36), $B = \sqrt{2}A$ and A is the (normalized) maximum amplitude of the matter wave at $t = 0$. The nonlinearity is either attractive or repulsive, and weak to moderate (cubic) or strong (quadratic). For simplicity, the absolute value of the nonlinear coefficient can be set to unity in both cases. For weak interactions [Eq. (6)], we can set $g_1 = 1$ by requiring that $L_0 = 2a_s\omega_\perp/\omega$. In addition, the nonlinear coefficient in the case of strong interactions can also be set to unity by setting $\omega = 9/(4\omega_\perp)$.

Typical examples of nonlinear accelerating matter waves are shown in Fig. 6. In particular, on the left and right columns of the figure, we set $b = 3/2$ and $b = 5/3$, leading to parabolic and cubic trajectories, respectively. In the second and third rows, the interactions are attractive, while in the fourth and fifth rows, the interactions are repulsive. In the top row of the figure, the linear dynamics are shown for comparison. A moderate cubic nonlinearity is used in the second and fourth rows, whereas a strong (quadratic) nonlinearity is used in the third and fifth rows. The main conclusion is that even in the case of relatively strong interactions, the BEC exhibits accelerating dynamics with a trajectory that remains almost invariant during propagation. Furthermore, in the case of strong attractive interactions, we note the tendency of the radiating part of the matter waves to organize in the form of localized soliton structures [Figs. 6(e) and 6(f)]. Another very interesting phenomenon in the case of attractive interactions that can be seen by comparing Figs. 6(a), 6(c), and 6(e) or Figs. 6(b), 6(d), and 6(f) is the increased acceleration, and thus the increased bending, of the nonlinear matter waves as compared to the linear ones. This increased acceleration is due to the interaction of the rays associated with the accelerating matter wave with the highly nonlinear part of the radiation (the solitons). On the other hand, in the case of repulsive interactions, the radiation spreads out and tends to equidistribute in space. Thus, its density remains relatively small and the interactions between the rays that form the accelerating matter wave and the radiation are reduced. As a result, its trajectory exhibits only minor differences in comparison to the trajectory of the linear matter wave.

V. CONCLUSIONS

We have shown that Bose-Einstein condensates can self-accelerate and abruptly autofocus without the presence of an external potential. Such matter waves can follow arbitrary power-law trajectories and can also take the form of the diffraction-free Airy wave that follows a parabolic trajectory. We suggested several different configurations to prepare such self-accelerating matter waves using standard atom

manipulation techniques with lasers or magnetic mirrors and lenses. Nonlinear dynamics of matter waves for both attractive and repulsive interactions in the cases of either weak-to-moderate or strong atom interactions has been analyzed.

ACKNOWLEDGMENTS

This work is supported by the action "ARISTEIA" (Grant No. 1261) in the context of the Operational Programme "Education and Lifelong Learning" that is co-funded by the European Social Fund and National Resources and by the Research Project ANEMOS co-financed by the European Union (European Social Fund - ESF) and Greek national funds through the Operational Program "Education and Lifelong Learning" of the National Strategic Reference Framework (NSRF) - Research Funding Program: Thales. W.K. acknowledges the financial support of the Future and Emerging Technologies (FET) programme within the 7th Framework Programme for Research of the European Commission, under FET Grant No. FP7-ICT-601180 (Matter Wave).

[1] S. Bose, Z. Phys. **26**, 178 (1924).
[2] A. Einstein, Sitzber. Kgl. Preuss. Akad. Wiss., 3 (1925).
[3] M. H. Anderson, J. R. Ensher, M. R. Matthews, C. E. Wieman, and E. A. Cornell, Science **269**, 198 (1995).
[4] K. B. Davis, M. O. Mewes, M. R. Andrews, N. J. van Druten, D. S. Durfee, D. M. Kurn, and W. Ketterle, Phys. Rev. Lett. **75**, 3969 (1995).
[5] T. M. Roach, H. Abele, M. G. Boshier, H. L. Grossman, K. P. Zetie, and E. A. Hinds, Phys. Rev. Lett. **75**, 629 (1995).
[6] E. A. Cornell, C. Monroe, and C. E. Wieman, Phys. Rev. Lett. **67**, 2439 (1991).
[7] E. Maréchal, S. Guibal, J.-L. Bossennec, R. Barbé, J.-C. Keller, and O. Gorceix, Phys. Rev. A **59**, 4636 (1999).
[8] E. A. Hinds and I. G. Hughes, J. Phys. D: Appl. Phys. **32**, R119 (1999).
[9] A. Smerzi, S. Fantoni, S. Giovanazzi, and S. R. Shenoy, Phys. Rev. Lett. **79**, 4950 (1997).
[10] I. Lesanovsky and W. von Klitzing, Phys. Rev. Lett. **99**, 083001 (2007).
[11] A. Trombettoni and A. Smerzi, Phys. Rev. Lett. **86**, 2353 (2001).
[12] J. Denschlag, J. E. Simsarian, D. L. Feder, C. W. Clark, L. A. Collins, J. Cubizolles, L. Deng, E. W. Hagley, K. Helmerson, W. P. Reinhardt, S. L. Rolston, B. I. Schneider, and W. D. Phillips, Science **287**, 97 (2000).
[13] A. E. Leanhardt, A. Görlitz, A. P. Chikkatur, D. Kielpinski, Y. Shin, D. E. Pritchard, and W. Ketterle, Phys. Rev. Lett. **89**, 190403 (2002).
[14] M. V. Berry and N. L. Balazs, Am. J. Phys. **47**, 264 (1979).
[15] K. Unnikrishnan and A. R. P. Rau, Am. J. Phys. **64**, 1034 (1996).
[16] G. A. Siviloglou and D. N. Christodoulides, Opt. Lett. **32**, 979 (2007).
[17] I. Kaminer, R. Bekenstein, J. Nemirovsky, and M. Segev, Phys. Rev. Lett. **108**, 163901 (2012).
[18] I. D. Chremmos, Z. Chen, D. N. Christodoulides, and N. K. Efremidis, Opt. Lett. **37**, 5003 (2012).
[19] J. Zhao, P. Zhang, D. Deng, J. Liu, Y. Gao, I. D. Chremmos, N. K. Efremidis, D. N. Christodoulides, and Z. Chen, Opt. Lett. **38**, 498 (2013).
[20] J. Giannini and R. Joseph, Phys. Lett. A **141**, 417 (1989).
[21] I. Kaminer, M. Segev, and D. N. Christodoulides, Phys. Rev. Lett. **106**, 213903 (2011).
[22] Y. Fattal, A. Rudnick, and D. M. Marom, Opt. Express **19**, 17298 (2011).
[23] P. Polynkin, M. Kolesik, J. V. Moloney, G. A. Siviloglou, and D. N. Christodoulides, Science **324**, 229 (2009).
[24] J. Baumgartl, M. Mazilu, and K. Dholakia, Nat. Photon. **2**, 675 (2008).
[25] Y. Hu, G. Siviloglou, P. Zhang, N. Efremidis, D. Christodoulides, and Z. Chen, in *Nonlinear Photonics and Novel Optical Phenomena*, edited by Z. Chen and R. Morandotti, Springer Series in Optical Sciences, Vol. 170 (Springer, New York, 2012), pp. 1–46.
[26] N. K. Efremidis and D. N. Christodoulides, Opt. Lett. **35**, 4045 (2010).
[27] D. G. Papazoglou, N. K. Efremidis, D. N. Christodoulides, and S. Tzortzakis, Opt. Lett. **36**, 1842 (2011).
[28] P. Zhang, J. Prakash, Z. Zhang, M. S. Mills, N. K. Efremidis, D. N. Christodoulides, and Z. Chen, Opt. Lett. **36**, 2883 (2011).
[29] I. Chremmos, N. K. Efremidis, and D. N. Christodoulides, Opt. Lett. **36**, 1890 (2011).
[30] I. D. Chremmos, Z. Chen, D. N. Christodoulides, and N. K. Efremidis, Phys. Rev. A **85**, 023828 (2012).
[31] V. M. Pérez-García, H. Michinel, and H. Herrero, Phys. Rev. A **57**, 3837 (1998).
[32] L. Salasnich, A. Parola, and L. Reatto, Phys. Rev. A **65**, 043614 (2002).
[33] N. K. Efremidis and D. N. Christodoulides, Phys. Rev. A **67**, 063608 (2003).
[34] P. Engels, I. Coddington, P. C. Haljan, V. Schweikhard, and E. A. Cornell, Phys. Rev. Lett. **90**, 170405 (2003).
[35] I. Shvarchuck, C. Buggle, D. S. Petrov, K. Dieckmann, M. Zielonkowski, M. Kemmann, T. G. Tiecke, W. von Klitzing, G. V. Shlyapnikov, and J. T. M. Walraven, Phys. Rev. Lett. **89**, 270404 (2002).